On The Diffusion of Sticky Particles in 1-D

Joshua DM Hellier* and Graeme J Ackland†
SUPA, School of Physics and Astronomy, University of Edinburgh, Mayfield Road, Edinburgh EH9 3JZ, United Kingdom
(Dated: May 25, 2018)

The 1D Ising model is the simplest Hamiltonian-based model in statistical mechanics. The simplest interacting particle process is the Symmetric Exclusion Process (SEP), a 1D lattice gas of particles that hop symmetrically and cannot overlap. Combining the two gives a model for sticky particle diffusion, SPM, which is described here. SPM dynamics are based on SEP with short-range interactions, allowing flow due to non-equilibrium boundary conditions. We prove that SPM is also a detailed-balance respecting, particle-conserving, Monte Carlo description of the Ising model. Neither the Ising model nor SEP have a phase transition in 1D, but the SPM exhibits a non-equilibrium transition. This transition is from normal diffusion to a state with close-to-zero flow, breaking into a two-phase mixture. We present a fully non-linear, analytic, mean-field solution, which has a crossover from a positive to a negative diffusion constant coincident with the full SPM transition. Thus, the mean field theory successfully predicts its own demise. The simplicity of the model suggests a wide range of possible applications.

Lattice gases are a ubiquitous tool for modeling complex systems from biology to traffic [1–7]. Analytically solvable cases involve non-interacting or excluding particles, but in any real system of interest, the moving objects interact. Many models tackle the situation where the diffusing objects interact with an external field or the substrate [8–13], and non-trivial flow is induced by these non-equilibrium interactions.

For many applications, one is interested in a system where the only non-equilibrium feature is a driving force applied at the boundaries, such as a chemical potential difference, while far from the boundaries the system is free to self-organize due to interactions between the particles. Surprisingly, there are few such models in the literature. One reason for this is that the interactions introduce nonlinearities in analytical models, which makes them challenging to solve, at least outside of limits in which they can be linearized. This is unfortunate because it is precisely these nonlinearities which introduce interesting behaviors such as discontinuities at the oxide-metal interface or diffusion instability [14, 15].

Here we investigate a simple one-dimensional flow model with interparticle interactions, the "Sticky Particle Model" (SPM), specified in the top left inset of Fig. 1.

There are many examples of models of driven-dissipative dynamics. It is sometimes assumed that locally non-equilibrium dynamics are required to model complex flows. The novel feature of SPM is that it has locally homogeneous equilibrium dynamics (i.e. it obeys detailed balance, has no external field, and has no interaction with the substrate). Nevertheless, it exhibits a nonequilibrium phase transformation from a homogeneous, diffusing phase to a jammed structure. We thereby demonstrate that while local dissipation or substrate interactions can cause non-diffusive flow, they are not a necessary requirement.

The SPM is based upon the symmetric exclusion process [16–21], augmented by an interaction rule which specifies that adjacent particles separate with rate λ instead of their normal hopping rate, 1. The quantity λ parametrizes the "stickiness" of the particles; when $\lambda > 1$, there is a tendency for particles to repel, whilst $\lambda < 1$ represents attraction. We prove in the supplementary materials that the rates specified in Fig. 1 obey detailed balance, with a Hamiltonian isomorphic to the Ising model.

One might contrast this approach (making a simple microscopic model and trying to learn from it about large-scale interface growth) with continuum approaches such as the KPZ equation [22–24] where one analyses the extreme large-scale dynamics using universality classes. The particle-conserving dynamics of SPM are like those used to analyze the equilibrium Ising model by Kawasaki [25]. SPM can be viewed as a simplified KLS model [26–28] in 1-dimension without an applied field. The KLS model has very interesting behaviour attributed to the applied field; however, we shall show that our simplified, symmetric model also exhibits complex unexpected behavior when driven by a chemical potential difference at the boundary.

Numerical simulation reveals the wide range of the SPM behaviors, such as those shown in Fig. 4. We will discuss these numerical results in more detail later, but first let us analyze the model analytically. Because of the interactions, the types of methods used for the full analytic solution of SEP cannot be applied; thus we pursue a mean-field theory approximation.

Let the spacing between lattice sites be a, let τ_0 be the free-particle hopping timescale, and the time-averaged (or ensemble-averaged, assuming ergodicity) occupation probability of the i^{th} lattice site be ρ_i. We introduce $\zeta = 1 - \lambda$ here for convenience: high ζ implies sticky particles, negative ζ implies repulsion. It is demonstrated in the supplementary materials that, in mean-field approx-

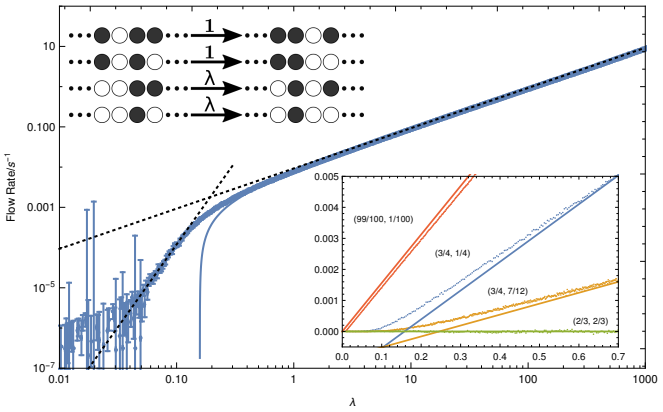

FIG. 1. **Top left:** SPM dynamics: White circles indicate particles, dark circles indicate empty sites (vacancies). Particles randomly move into adjacent vacancies with rate 1, unless there is an adjacent particle, in which case they move with rate λ; the state of the site beyond the new position is irrelevant. Particles can move left or right, such that the whole model is totally symmetric.
Bottom right: Mean flow rate as a function of λ with fixed boundary densities (ρ_0, ρ_L) as labeled in the plot. The MFT predictions are indicated by the solid line. Each data point is derived from systems of length 64 (length 32, 128 and 256 give similar results), each using over 10^8 Gillespie steps: 4×10^5 for equilibration, followed by 10^4 measurement runs of 10^3 steps interspersed with 16000 decorrelation steps. The 10^4 uncorrelated samples allow us to measure accurate flow rates and densities and the statistical distributions of both quantities; flow moments and the density data are given as supplementary materials.
Main figure: Log-log plot of the $\left(\frac{3}{4}, \frac{1}{4}\right)$ data, extended over many orders of magnitude of λ. The dashed lines represent asymptotic power-laws; the higher-λ one matches the mean-field, diffusion-limit prediction (solid line) with flow $\propto \lambda^1$, whilst the lower-λ one - fitted in the range $0.04 \leq \lambda \leq 0.1$ - shows critically-slowed flow with flow $\propto \lambda^4$.

imation regime,

$$\tau_0 \frac{\partial \rho_i}{\partial t} = (1-\rho_i)\left[(1-\zeta\rho_{i-2})\,\rho_{i-1} + (1-\zeta\rho_{i+2})\,\rho_{i+1}\right] - \rho_i\left[2\zeta\rho_{i-1}\rho_{i+1} - (3-\zeta)\,(\rho_{i-1}+\rho_{i+1}) + 2\right]. \quad (1)$$

Switching to the continuum limit by taking $a \to 0$, and neglecting $\mathcal{O}(a^4)$ terms, we may re-express this as a conserved flow J as follows:

$$\frac{\partial \rho}{\partial t} = -\frac{\partial J}{\partial x}, \quad (2)$$

$$J = -D(\rho)\frac{\partial \rho}{\partial x}, \quad (3)$$

$$D(\rho) = \frac{a^2}{\tau_0}\left[1 - \zeta\rho\,(4-3\rho)\right]. \quad (4)$$

Thus, the MFT says that the particles should diffuse with a diffusion coefficient $D(\rho)$ which depends upon the local density, and exhibits an unexpected symmetry about $\rho = \frac{2}{3}$.

In order to understand the implications of the MFT, let us consider some limits. As $\zeta \to 0$ (i.e. as the model becomes a simple exclusion model), $D \to \frac{a^2}{\tau_0}$. Likewise, in the dilute limit $\rho \to 0$, $D \to \frac{a^2}{\tau_0}$, reflecting the fact that the interactions become irrelevant as particles never meet. Conversely, in the full limit $\rho \to 1$, $D \to \frac{\lambda a^2}{\tau_0}$; we now have a dilute gas of vacancies, which hop with rate $\frac{\lambda}{\tau_0}$. One may observe that equation 4 has a symmetry under $\rho \mapsto \frac{4}{3} - \rho$; thus, the dynamics should be symmetric under a density profile reflection around $\rho = \frac{2}{3}$. This is where D always attains its extremal value, $\frac{a^2}{\tau_0}\left[1 - \frac{4}{3}\zeta\right]$; hence for $\zeta > 3/4$ the MFT diffusion coefficient becomes negative in regions with $\frac{2}{3} - \frac{\sqrt{\zeta(4\zeta-3)}}{3\zeta} < \rho < \frac{2}{3} + \frac{\sqrt{\zeta(4\zeta-3)}}{3\zeta}$. Finally, solutions to the continuum MFT containing domains with a negative diffusion coefficient are linearly unstable; thus, if $D_{MFT}(\rho) < 0$, ρ itself is unstable with respect to either of the two densities for which $D(\rho) \sim 0$ (see SM for proof). Instead of observing "backwards diffusion" we would see an extremely slow flow or no flow at all. The MFT implies that the transition to this critically slowly-flowing regime happens suddenly, like a phase transition: this can be checked with numerics.

It is possible to solve the continuum MFT in a steady state on a finite domain, say $x \in (0, L)$. The continuity equation implies that $J(x) = J_0 = \text{const.}$, and by integrating both sides of this equation with respect to x we find that

$$J(x) = (x - x_0)J_0 = -\frac{a^2}{\tau_0}\rho\left[1 + \zeta\rho\,(\rho - 2)\right], \quad (5)$$

a cubic equation which can be solved to give $\rho(x)$ with appropriately chosen real constant x_0. If we impose Dirichlet boundary conditions on this system, say $\rho(0) = \rho_0$ and $\rho(L) = \rho_L$, we find that

$$J_0 = \frac{a^2}{L\tau_0}\left[\rho_0 - \rho_L + \zeta\left(\rho_0\left[\rho_0^2 - 2\right] - \rho_L\left[\rho_L^2 - 2\right]\right)\right]. \quad (6)$$

We may consider applying small concentration gradients across a domain by setting $\rho_0 = \rho_M + \frac{1}{2}\delta\rho$ and $\rho_L = \rho_M - \frac{1}{2}\delta\rho$. Doing so, we find that the effective diffusion coefficient of the domain $D_{\text{Eff}} = L\frac{\partial J}{\partial \delta\rho}\big|_{\delta\rho=0}$ obeys

$$D_{\text{Eff}} = \frac{a^2}{\tau_0}\left[1 - \zeta\rho_M(4 - 3\rho_M)\right], \quad (7)$$

which implies the same symmetry about $\rho = \frac{2}{3}$ and negative flow region as Eq. 4

We implemented the SPM numerically using the Gillespie algorithm [29–31] implemented in the `KMCLib` [32] Kinetic Monte Carlo package. The codes are publicly available [33]. With periodic boundary conditions, we recover the fixed magnetization Ising Model, as expected.

To investigate flow, we set up a chemical potential difference across the system by defining the boundaries. We use two boundary-layer lattice sites which switch between being full and empty such that their time-averaged occupation matches the desired concentration; there are then chances for particles to appear and disappear at these boundary layers, as well as migrate into the main part of the system. These boundary conditions reproduce the effect of having particle reservoirs attached to the edges of the domain, which we verified by inspecting the time-averaged occupations of sites near the boundary.

We have used the setup above to explore three scenarios, discussed in the following sections. In each of these we refer to a boundary condition configuration by (ρ_0, ρ_L), with ρ_0 and ρ_L being the boundary densities at opposite ends of the system of length L. We measure overall particle flow rate from the number of particles entering and leaving, and maintain a histogram of the distribution of the number of particles in the system. Our initial configurations have randomly distributed particles with density $\frac{1}{2}(\rho_0 + \rho_L)$, and we then run the system for a sufficient number of equilibration steps to destroy any initial transients.

The MFT suggested that a transition from a steady flow regime to a critically slow flow regime might occur as the stickiness varies. We test for this by measuring the particle density as well as the mean, variance and skewness of the flow rate as a function of λ for fixed (ρ_0, ρ_L). If such a transition does indeed occur, we should expect to see something interesting happen as λ passes through the transition point.

Fig. 1 shows a log-log plot of flow rate over a large range of λ for fixed boundary conditions. The inset shows the effect of boundary conditions. The equivalent MFT results are calculated using Eq. 6, which is predicted to break down when $\lambda \sim \frac{1}{4}$, below which the MFT flow becomes negative. The simulated SPM flow does continue, at a much reduced rate and with different power-law behavior from particle diffusion. This different flow behavior defines the SPM transition. For low-stickiness ($\lambda > \frac{1}{4}$) the MFT is in very good agreement with the simulations, and this continues for repulsive $\lambda >> 1$, where the mean flow rate varies linearly with λ.

For very high stickiness ($\lambda < 0.04$), convergence is very slow, hence the large standard errors. However, there is a regime when $0.04 \leq \lambda \leq 0.1$ where the mean flow displays clear $\mathcal{O}(\lambda^4)$ power-law behaviour. Defining the SPM transition by where the power laws cross at $\lambda = 0.194$, gives good agreement with the MFT transition to negative flow. The key point here is that as that as we pass from high-λ to low-λ, the scaling in λ does change, which suggests to us that the mechanism by which material is transferred through the medium changes from the standard diffusive one (which is well-described by the MFT) to something different, which to our knowledge has not been previously observed. In this region the MFT assumption of $\rho \sim \rho_M = \frac{1}{2}(\rho_0 + \rho_L)$ has broken down, and the number of particles in the system increases (see SM). We can interpret the critically slow flow as being due to rare-event fluctuations in an otherwise full region.

In Fig. 2 we show the effect of varying both the driving force ($\delta\rho$) and stickiness (λ), using boundaries $(\rho_0, \rho_L) = (\rho_M + \frac{1}{2}\delta\rho, \rho_M - \frac{1}{2}\delta\rho)$ for fixed ρ_M. The MFT prediction for the mean flow is again a good fit until λ becomes sufficiently sticky, when the flow becomes critically slow, manifesting as zero flow plus noise in Fig. 2(b). The density within the system is very close to ρ_M until λ drops below 1/4, at which point parts of the system fill ($\rho \sim 1$).

FIG. 2. Flow rate mean observed when varying the difference $\delta\rho$ between the boundary concentrations $(\rho_0, \rho_L) = (\rho_M + \frac{1}{2}\delta\rho, \rho_M - \frac{1}{2}\delta\rho)$ and λ (The top panel is the MFT prediction for the flow rate, whilst bottom shows the observed mean flow rate). We chose $\rho_M = \frac{1}{2}$, as this gives us the biggest range of $\delta\rho$ to investigate. These calculations were performed with the same run parameters (system length etc) as above.

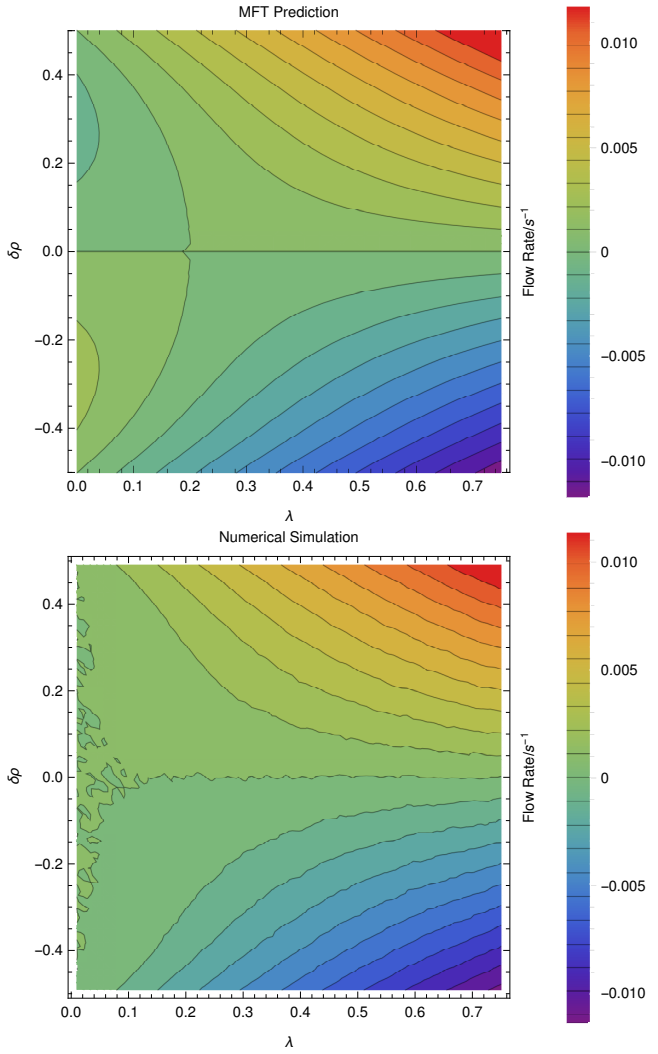

For relatively small driving force $\delta\rho$, we find J varies

approximately linearly with $\delta\rho$, thus we can define $D_{\mathrm{Eff}} = \frac{\partial J}{\partial \delta\rho}\big|_{\delta\rho=0}$, the effective diffusion coefficient and measure it using linear regression.

FIG. 3. Comparison of effective diffusion coefficient D in the MFT (top) and in direct simulation (bottom) as a function of density and stickiness. The region where MFT gives negative diffusion is represented as $D = 0$. The simulations used 124 sites averaged over $\sim 10^9$ steps at each of $12 \times 24 \times 16$ $(\lambda, \rho_M, \delta\rho)$ combinations. Full details in the supplementary materials.

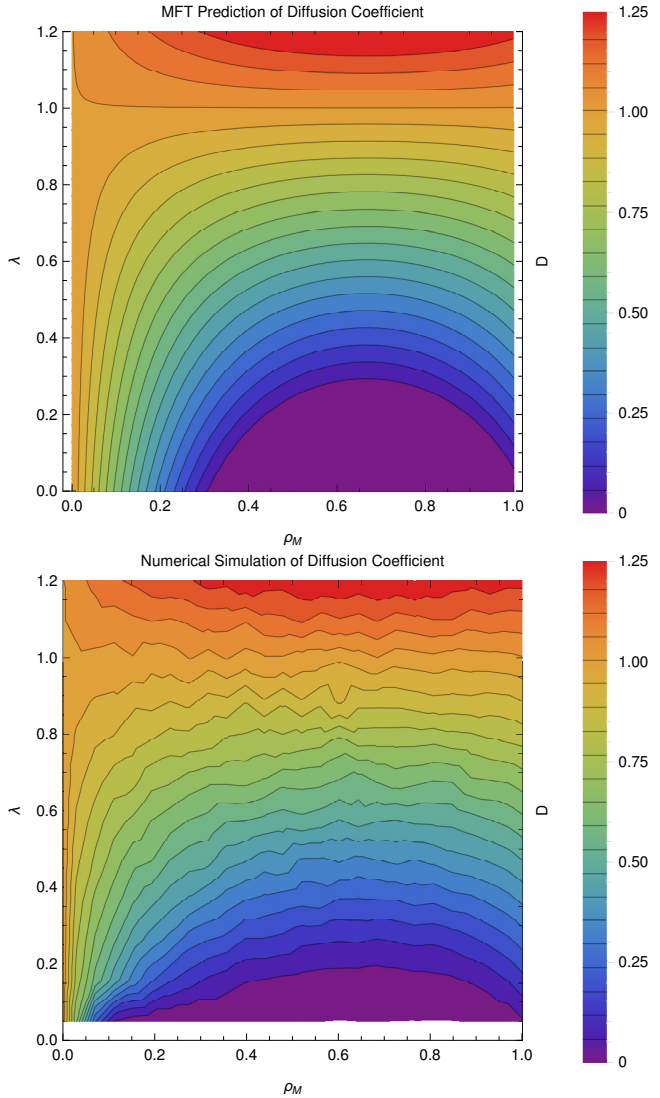

In Fig 3 we compare the measured diffusion coefficient with the MFT result (Eq. 7) The MFT and simulation agree well for low stickiness, and both show the maximum D at $\rho_M = \frac{2}{3}$. For high stickiness, where the MFT prediction gives a negative diffusion constant, measurement gives very low positive values for the current, making the determination of D difficult; however, the important thing to note is that this critically slow flow corresponds to the the negative-D region predicted by the MFT (indicated in purple).

It is instructive to get an overview of how the SPM particles move during flow. Fig. 4 shows a plot of the flow structure in an interesting regime. Over short timescales little structure is visible, the dynamics appearing as a random walk with some tendency for particles to clump; over longer timescales the diffusive behavior is more evident, with a textured structure suggesting characteristic velocity of particles or vacancies through emergent correlated clumps. In the limiting case of low λ the density of particles in the system tends to 1, irrespective of boundary density: this may be because the interactions between particles are strong enough that the filled state has lower chemical potential than either boundary. Another interesting case is the limit of high λ, where irrespective of boundary density, the internal density tends to $\rho = \frac{2}{3}$, the value which gives maximal flow and maximum entropy production. Additional plots can be found in the supplementary materials.

FIG. 4. Indicative spacetime flow pattern for sticky free-flow $\left[\lambda = \frac{3}{20}, (\rho_0, \rho_L) = (\frac{3}{4}, \frac{1}{4})\right]$; other combinations shown in the supplementary materials. Time runs along the x-axis, space (1 pixel=1 site) along the y-axis, with grayscale tone (black being empty, white being full) illustrating average site occupation over (clockwise from top left) $\frac{1}{32}$, 1, 8 and 32 Gillespie steps per site respectively.

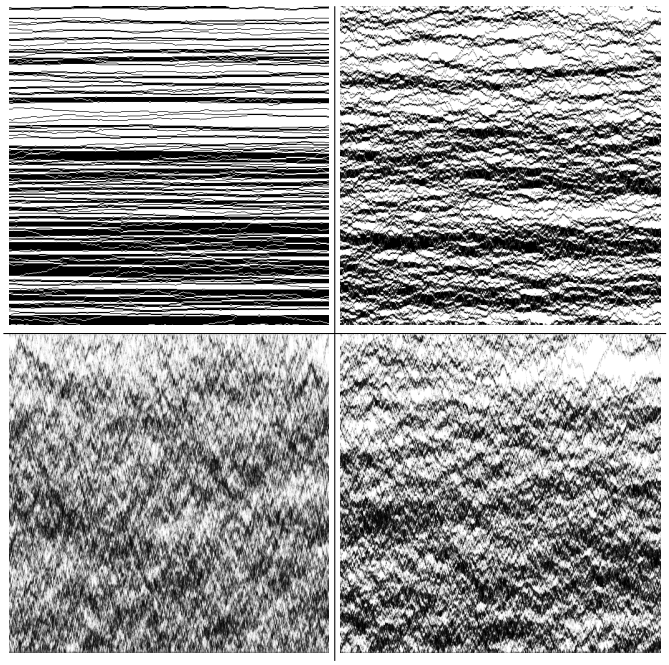

To conclude, we have solved a nonlinear model for self-interacting sticky particles diffusing in 1D. Although only the particles exhibit stickiness, the analytics suggest a symmetry between vacancy-type and particle-type flow at density of $\frac{2}{3}$, which is observed in the simulation. The flow exhibits a foamy pattern with intermediate time-and-space correlations. The continuum solution MFT is a good predictor of the bulk flow behavior of the

SPM. The negative diffusion constant found in MFT at high stickiness indicates that the assumption of homogeneous density break down: thus the MFT predicts its own demise, and this agrees well with our numerics.

We would like to thank EPSRC (student grant 1527137) and Wolfson Foundation for providing the funding, Mikael Leetmaa for producing `KMCLib`, and the `Eddie3` team here at Edinburgh for maintaining the hardware used. We would also like to thank Martin Evans, Bartek Waclaw and Richard Blythe for some very helpful discussions during the production of this letter.

* J.D.M.Hellier@sms.ed.ac.uk
† G.J.Ackland@ed.ac.uk

[1] V. Belitsky and G. M. Schütz, Journal of Statistical Mechanics: Theory and Experiment **2011**, P07007 (2011).
[2] M. Mobilia, I. T. Georgiev, and U. C. Täuber, Journal of Statistical Physics **128**, 447 (2007).
[3] B. Tegner, L. Zhu, C. Siemers, K. Saksl, and G. Ackland, Journal of alloys and compounds **643**, 100 (2015).
[4] L. Zhu, Q.-M. Hu, R. Yang, and G. Ackland, Journal of Physical Chemistry C **116**, 24201 (2012).
[5] B. E. Deal and A. S. Grove, Journal of Applied Physics **36**, 3770 (1965), https://doi.org/10.1063/1.1713945.
[6] N. Cabrera and N. F. Mott, Reports on Progress in Physics **12**, 163 (1949).
[7] S. Buzzaccaro, R. Rusconi, and R. Piazza, Phys. Rev. Lett. **99**, 098301 (2007).
[8] A. J. C. Ladd, M. E. Colvin, and D. Frenkel, Phys. Rev. Lett. **60**, 975 (1988).
[9] T. M. Liggett, *Interacting particle systems* (Springer-Verlag, Berlin, 1985).
[10] E. Ben-Naim, S. Y. Chen, G. D. Doolen, and S. Redner, Phys. Rev. Lett. **83**, 4069 (1999).
[11] S. F. Shandarin and Y. B. Zeldovich, Rev. Mod. Phys. **61**, 185 (1989).
[12] L. Frachebourg, Phys. Rev. Lett. **82**, 1502 (1999).
[13] L. Frachebourg, P. A. Martin, and J. Piasecki, Physica A Statistical Mechanics and its Applications **279**, 69 (2000), cond-mat/9911346.
[14] V. V. Obukhovsky, A. M. Kutsyk, V. V. Nikonova, and O. O. Ilchenko, Phys. Rev. E **95**, 022133 (2017).
[15] N. V. Gorokhova and O. E. Melnik, Fluid Dynamics **45**, 679 (2010).
[16] K. E. P. Sugden and M. R. Evans, Journal of Statistical Mechanics: Theory and Experiment **2007**, P11013 (2007).
[17] M. Kollmann, Phys. Rev. Lett. **90**, 180602 (2003).
[18] B. Lin, M. Meron, B. Cui, S. A. Rice, and H. Diamant, Phys. Rev. Lett. **94**, 216001 (2005).
[19] C. Hegde, S. Sabhapandit, and A. Dhar, Phys. Rev. Lett. **113**, 120601 (2014).
[20] P. L. Krapivsky, K. Mallick, and T. Sadhu, Phys. Rev. Lett. **113**, 078101 (2014).
[21] T. Imamura, K. Mallick, and T. Sasamoto, Phys. Rev. Lett. **118**, 160601 (2017).
[22] M. Kardar, G. Parisi, and Y.-C. Zhang, Phys. Rev. Lett. **56**, 889 (1986).
[23] J. Krug and H. Spohn, Phys. Rev. A **38**, 4271 (1988).
[24] T. Sasamoto and H. Spohn, Phys. Rev. Lett. **104**, 230602 (2010).
[25] K. Kawasaki, Phys. Rev. **145**, 224 (1966).
[26] S. Katz, J. L. Lebowitz, and H. Spohn, Journal of Statistical Physics **34**, 497 (1984).
[27] R. K. P. Zia, Journal of Statistical Physics **138**, 20 (2010).
[28] Y. Kafri, E. Levine, D. Mukamel, G. M. Schütz, and R. D. Willmann, Phys. Rev. E **68**, 035101 (2003).
[29] D. T. Gillespie, The Journal of Physical Chemistry **81**, 2340 (1977), http://dx.doi.org/10.1021/j100540a008.
[30] A. Bortz, M. Kalos, and J. Lebowitz, Journal of Computational Physics **17**, 10 (1975).
[31] A. Prados, J. J. Brey, and B. Sánchez-Rey, Journal of Statistical Physics **89**, 709 (1997).
[32] M. Leetmaa and N. V. Skorodumova, Computer Physics Communications **185**, 2340 (2014), arXiv:1405.1221 [physics.comp-ph].
[33] J. Hellier, (2018), 10.5281/zenodo.1162818.